Journal of Quantitative Spectroscopy & Radiative Transfer 292 (2022) 108366

Contents lists available at ScienceDirect

Journal of Quantitative Spectroscopy & Radiative Transfer

journal homepage: www.elsevier.com/locate/jqsrt

A coupled-channel deperturbation treatment of the $X^2\Sigma^+ \sim A^2\Pi \sim B^2\Sigma^+$ complex of the CN radical towards spectroscopic accuracy

V.A. Terashkevich[a], E.A. Pazyuk[a], A.V. Stolyarov[a,*], S.N. Yurchenko[b]

[a] Department of Chemistry, Lomonosov Moscow State University, Moscow, 119991, Leninskie gory 1/3, Russia
[b] Department of Physics and Astronomy, University College London, Gower St, London WC1E 6BT, UK

ARTICLE INFO

Article history:
Received 10 July 2022
Revised 2 September 2022
Accepted 2 September 2022
Available online 6 September 2022

Keywords:
CN radical
Electronic states
Deperturbation analysis
Coupled-channel approximation

ABSTRACT

A global deperturbation analysis of the experimental rovibronic term values of the $X^2\Sigma^+$, $A^2\Pi$ and $B^2\Sigma^+$ states of the $^{12}C^{14}N$ isotopomer has been performed. The inverse spectroscopic problem was directly solved in the framework of the reduced 4×4 coupled-channel (RCC) deperturbation model based on potential energy curves (PECs) as well as the spin-orbit and L-uncoupling electronic matrix elements between the $X^2\Sigma^+$, $A^2\Pi$, and $B^2\Sigma^+$ states. Regular perturbations of the $X\sim A\sim B$ complex by the remote doublet states manifold were taken into account by introducing of the fine-structure parameters as explicit functions of interatomic distance. The optimized PECs and non-adiabatic coupling functions describe the vast majority (5600–6570) of the empirical term values, attributed to locally and regularly perturbed levels of the complex, with a root-mean-squared deviation of 0.015-0.05 cm^{-1}, depending on a particular set of the experimental term values included in the fitting procedure. The resulting mass-invariant RCC deperturbation parameters can straightforwardly extend a line-list of all CN isotopomers into a wide region of vibrational and rotational quantum numbers.

1. Introduction

The diatomic CN radical, known, primarily, as one of the first molecules to be discovered in the interstellar medium (ISM) [1], is an object of persistent interest in the fields of astrophysics and astrochemistry. At the moment, the energies, radiative, collisional, and magnetic properties of the gas-phase CN radical are utilized in solving key questions in the realm of astronomical applications such as measurements of the background radiation temperature [2]; determination of the chemical composition and time evolution of comet comas [3]; modeling of stellar nucleosynthesis [4], including carbon and nitrogen abundance and their isotopic ratios; the radiative association and cooling occurring during the collisions of C and N atoms [5]; and probing into the possible variation of fundamental (dimensionless) physical constants on the cosmological time scale [6]. The relative intensity distribution in strong emission band spectra of the CN radical is widely used in non-contact (optical) temperature measurements of its flame and plasma [7]. In particular, laser-induced breakdown spectroscopy (LIBS) often exploits the "violet" ($B^2\Sigma^+ - X^2\Sigma^+$) band system of the CN radical for carbon atom analysis of organic compounds in air [8,9].

The permanent, long, and successful history of the spectroscopic study of the CN radical in the ultra-violet, infra-red, and microwave regions has led to the accumulation of a huge, but not comprehensive, line-list of experimental rovibronic transitions, the overwhelming majority of which are related to the lowest three electronic states: $X^2\Sigma^+$, $A^2\Pi$, and $B^2\Sigma^+$ (see Fig. 1). The measured active rotational-vibrational energy levels (MARVEL) approach [10] has been recently applied in order to accomplish a the statistically substantiated translation of the measured lines positions to the corresponding rovibronic term values. The MARVEL procedure, which is independent of the spectroscopic model, yielded about 6860 empirical term values covering the $v_X \in [0, 18]$, $v_A \in [0, 22]$, and $v_B \in [0, 19]$ vibrational levels of the $X^2\Sigma^+ \sim A^2\Pi \sim B^2\Sigma^+$ complex for the naturally most abundant $^{12}C^{14}N$ isotopologue [11].

All vibrational levels belonging to the $X\sim A\sim B$ complex (including the lowest terms of the ground state) undergo *regular* rotational e/f-parity perturbations caused by a combination of the spin-orbit (SO) and L-uncoupling intramolecular interactions with the remote doublet and quartet states manifold. These, normally weak, perturbations appear in the observed spectra as the, so-

* Corresponding author.
E-mail address: avstol@phys.chem.msu.ru (A.V. Stolyarov).

https://doi.org/10.1016/j.jqsrt.2022.108366
0022-4073/

Table 1
The RMSD obtained for the three experimental data sets (`set I-III`) of the refined MARVEL [11] rovibronic term values for the $X^2\Sigma^+ \sim A^2\Pi \sim B^2\Sigma^+$ complex of the most abundant $^{12}C^{14}N$ isotopologue. $ZPE_{fit}=1031.060+\delta_{ZPE}$ is the empirical zero-point-energy which corresponds to the minimum of the ground $X^2\Sigma^+$ PEC. The δ_{ZPE}-value is treated here as a small correction to be adjusted during the fit. The ZPE_{CC} is the CC energy evaluated by means of the corresponding set of the deperturbed molecular parameters. All energies are given in cm^{-1}.

Set	v_X^{max}	v_A^{max}	v_B^{max}	$N^{exp}_{total/fit}$	RMSD	δ_{ZPE}	ZPE_{fit}	$ZPE_{fit} - ZPE_{CC}$
I	12	16	10	5620/5608	0.015	0.075	1031.135	0.012
II	18	22	12	6483/6311	0.030	0.086	1031.146	-0.003
III	18	22	19	6838/6566	0.050	0.090	1031.150	0.025

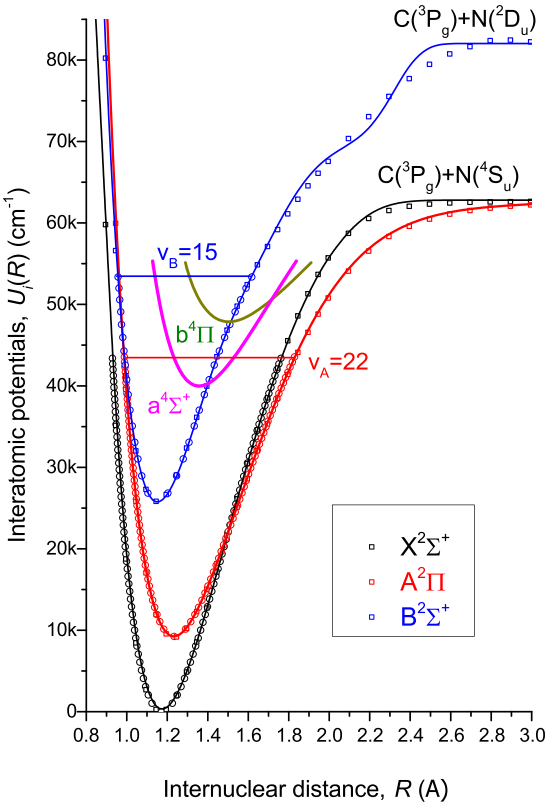

Fig. 1. The empirical and *ab initio* PECs for $X^2\Sigma^+$, $A^2\Pi$, and $B^2\Sigma^+$ states of the CN radical. The solid lines represent the EMO potentials obtained in the present work using the `set-II` (see Table 1 for details) of the MARVEL experimental term values [10]. The open squares are *ab initio* potentials from Ref. [25]. The open circles represent the Rydberg-Klein-Rees (RKR) potentials constructed using the Dunham molecular constants from Refs. [18,26]. The *ab initio* potentials of the lowest quartet $a^4\Sigma^+$ and $b^4\Pi$ states are borrowed from Ref. [14].

called, σ and Λ-doubling effects [12,13], which monotonically increases as rotational excitation increases. Furthermore, some excited rovibronic levels of the $X \sim A \sim B$ complex undergo strong *local* perturbations caused by mutual SO and electronic-rotational interactions between close-lying (i.e. coincidentally almost degenerate) levels of the complex. The most pronounced perturbations involve levels belonging to the $B^2\Sigma^+$ state, as this excited state additionally interacts with the nearby "dark" quartet states manifold [14] (see Fig. 1).

These *local* perturbations were only partly deperturbed in Refs. [15,16], by employing the band-by-band version of the traditional Effective Hamiltonian approach (EHA) [17]. Regularly perturbed levels of the $X \sim A \sim B$ complex were, also, successfully treated in the framework of the conventional EHA providing a description of the line positions with almost experimental accuracy. The resulting deperturbed structure parameters of the $X^2\Sigma^+$, $A^2\Pi$, and $B^2\Sigma^+$ states were then combined with the *ab initio* $B-X$, $B-A$ and $A-X$ transition dipole moments to generate a Molecular Line Lists, Intensities and Spectra (MoLLIST) for the $X \sim A \sim B$ complex [18] using the LEVEL [19] and PGOPHER [20] programs.

Unfortunately, the traditional EHA normally reproduces *local* and *regular* perturbations observed in a wide range of energy excitation with different levels of accuracy, neither of which reaches the experimental one. The EHA can interpolate missing lines with nearly the required spectroscopic accuracy, but does not predict spectra accurately outside the experimental region, because of the fundamental limitations of perturbation theory. However, employing an alternative coupled-channel (CC) spectroscopic model [13] will generally accomplish description of all perturbations with the same level of accuracy. The inverse CC method realized in the Duo program package [21] has been recently used to accomplish a global deperturbation analysis of the $X \sim A \sim B$ complex of CN [22]. However, the resulting molecular parameters of the reduced 4×4 coupled-channel (RCC) model [23], which included the adiabatic potential energy curves (PECs) of the coupled states, and the non-adiabatic spin-orbit and L-uncoupling matrix elements as functions of interatomic distance, r, was able to reproduce a whole set of experimental term values of the $X \sim A \sim B$ complex with root-mean-squared deviation (RMSD) of 0.05-1.0 cm^{-1}, which is more than an order of magnitude higher than the accuracy of the spectroscopic measurements.

In the present work, the overall accuracy of the 4×4 RCC deperturbation model implemented in [22] has been significantly improved by taking into account the numerous *regular* interactions of the remote doublet states manifold with the $X^2\Sigma^+ \sim A^2\Pi \sim B^2\Sigma^+$ complex. This has been realized, as in Ref. [24], by introducing the mass-invariant σ and Λ-doubling parameters and 2-nd order rotational non-adiabatic corrections as explicit radial functions of r. It is important that the introduced fine-structure functions are recently available from the high level *ab initio* electronic calculations [25], and some of them were used here to constrain a variation of the fitting parameters.

2. Deperturbation machinery

2.1. Modeling Hamiltonian

The rovibronic non-adiabatic energies $E^{e/f}$ (eigenvalues) and corresponding multi-component vibrational wave functions $\mathbf{\Phi}$ (eigenfunctions) were determined for both e- and f-parity levels of the $X^2\Sigma^+ \sim A^2\Pi \sim B^2\Sigma^+$ complex of CN radical by solving four coupled-channel equations [21]:

$$\left(-\mathbf{I}\frac{\hbar^2 d^2}{2\mu dr^2} + \mathbf{V}^{e/f}(r;\mu,J) - \mathbf{I}E^{e/f}\right)\mathbf{\Phi}(r) = 0. \quad (1)$$

The hyperfine structure of the doublet states was neglected, and the conventional boundary $\phi_i(0) = \phi_i(\infty) = 0$ and normalization $\sum_i P_i = 1$ conditions were used. Hereafter, $P_i = \langle\phi_i|\phi_i\rangle$ is the fractional partition of the non-adiabatic $X \sim A \sim B$ level and $i \in [X^2\Sigma^+, A^2\Pi_{1/2}, A^2\Pi_{3/2}, B^2\Sigma^+]$, $\mathbf{I}$ is the identity matrix, μ is

the reduced molecular mass, J is the rotational quantum number, $\mathbf{V}^{e/f}(r;\mu,J)$ - is the r-depending 4×4 matrix of potential energy.

The diagonal matrix elements of $\mathbf{V}^{e/f}(r;\mu,J)$ were specified in the form:

$$V^{e/f}_{X-X} = U_X + B[Y(Y\mp1)+\gamma_X(1\mp Y)] + B^2\left[q_X(1\mp Y)^2\right], \tag{2}$$

$$V^{e/f}_{A_{3/2}-A_{3/2}} = U_A + A^{so} + B\left[Y^2-2\right] + B^2\left[q_A(Y^2-1)+q_{A\Delta}(Y^2-4)\right], \tag{3}$$

$$V^{e/f}_{A_{1/2}-A_{1/2}} = U_A - A^{so} + B\left[Y^2+p_A(1\mp Y)\right] + B^2\left[q_A(1\mp Y)^2+q_{A\Delta}(Y^2-1)\right], \tag{4}$$

$$V^{e/f}_{B-B} = U_B + B[Y(Y\mp1)], \tag{5}$$

where

$$Y \equiv J+1/2; \qquad B \equiv \frac{\hbar^2}{2\mu r^2}.$$

The symbol $\mp$ refers to e- and f-parity rotational energy levels, respectively.

The non-vanishing off-diagonal matrix elements of $\mathbf{V}^{e/f}(r;\mu,J)$ were defined as

$$V^{e/f}_{A_{1/2}-A_{3/2}} = -B\left[1+\frac{p_A+p_{A\Delta}}{2}+Bq_A(1\mp Y)\right]\sqrt{Y^2-1}, \tag{6}$$

$$V^{e/f}_{A_{1/2}-X} = V^{so}_{AX} + BL_{AX}(1\mp Y); \quad V^{e/f}_{A_{3/2}-X} = -BL_{AX}\sqrt{Y^2-1}, \tag{7}$$

$$V^{e/f}_{A_{1/2}-B} = V^{so}_{AB} + BL_{AB}(1\mp Y); \quad V^{e/f}_{A_{3/2}-B} = -BL_{AB}\sqrt{Y^2-1}. \tag{8}$$

All electronic parameters in the 4×4 RCC deperturbation model above are tacitly assumed to be explicit functions of interatomic distance. In particular, $U_i(r)$ are the conventional adiabatic PECs of the isolated $i\in[X^2\Sigma^+, A^2\Pi, B^2\Sigma^+]$ states corresponding to the pure Hund's case "**a**"; $A^{so}(r)$ is the spin-orbit splitting function of the doublet $A^2\Pi$ state; $V^{so}_{AB}(r)$ and $V^{so}_{AX}(r)$ are the off-diagonal spin-orbit coupling matrix elements between the $A^2\Pi$ state and either the $X^2\Sigma^+$ or $B^2\Sigma^+$ states, whereas $L_{AB}(r)$ and $L_{AX}(r)$ are the analogous L-uncoupling (Coriolis) matrix elements.

A key characteristic of the present RCC treatment of the $X\sim A\sim B$ complex lies in accounting for the regular interactions of the complex with the remote doublet states manifold using the 2-nd order van-Vleck contact transformations [12]. This was accomplished by the introducing the, so-called, fine-structure parameters [13] as mass-independent functions of r into the RCC model [23,24]. For instance, the $\gamma_X(r)$ and $q_X(r)$ functions [27] in Eq. (2) are responsible for the SO and L-uncoupling interactions of the ground X-state with energetically higher $^2\Pi$ states, skipping the $A^2\Pi$ state. The $p_A(r)$ and $q_A(r)$ functions involved in Eqs. (3), (4) and (6) take into account the intramolecular perturbation of the $A^2\Pi$ state by the $^2\Sigma^\pm$ states manifold, excluding its energetically lowest members $X^2\Sigma^+$ and $B^2\Sigma^+$. The $p_{A\Delta}(r)$ and $q_{A\Delta}(r)$ functions arise from the interaction of the $A^2\Pi$ state with higher-lying $^2\Delta$ states.

A very similar RCC Hamiltonian, including the explicitly r-depending fine structure parameters, has been recently developed for the global deperturbation treatment of the lowest doublet states of nickel monohydride [24]. The explicit second order van-Vleck's formulae suitable for the evaluation of the fine-structure Λ-doubling parameters can be found elsewhere (see, for instance, Refs. [17,24,27,28]). It should be noted that the required SO and L-uncoupling electronic matrix elements between the low-lying doublet states of CN have recently become available from the relevant *ab initio* electronic structure calculations [5,22,25]. Furthermore, the Λ-doubling parameters obtained in [25] have demonstrated the surprisingly small contribution of the higher-lying $^2\Pi$ states into the $\gamma_B(r)$ and $q_B(r)$ functions of the excite $B^2\Sigma^+$ state compared to their impact on the ground state. This is the reason why the corresponding γ_B and q_B parameters were neglected in the modeling Hamiltonian above (compare Eq. (5) to Eq. (2)).

Importantly, the RCC deperturbation model described above has completely disregarded any impact of the highly excited quartet states manifold (see, Fig. 1) since both experimental [16,29,30] and *ab initio* [14] information available now is definitely not sufficient to perform unambiguous deperturbation analysis even the lowest $a^4\Sigma^+$ and $b^4\Pi$ states.

2.2. Approximation of the electronic parameters

The interatomic PECs, $U_i(r)$, for all three states of the $X\sim A\sim B$ complex were approximated using the analytical Extended Morse Oscillator (EMO) expression [31]:

$$U_i^{EMO}(r) = T_e + D_e\left[1-e^{-\beta(r)(r-r_e)}\right]^2, \tag{9}$$

where T_e is the electronic term, D_e is the dissociation energy, and r_e is the equilibrium distance. In contrast to the conventional Morse potential, the r-depending exponential coefficient, $\beta(r)$, in Eq. (9) is defined as the polynomial series:

$$\beta(r) = \sum_{i=0}^{N}\beta_i[y_p(r)]^i, \tag{10}$$

of the reduced coordinate [32]

$$y_p(r) = \frac{r^p - r^p_{\rm ref}}{r^p + r^p_{\rm ref}}; \quad y_p\in[-1;1], \tag{11}$$

where p is as integer number and $r_{\rm ref}$ is the reference distance.

Both on-diagonal ((3)–(4)) and off-diagonal ((6)–(8)) SO and L-uncoupling electronic matrix elements between the $X^2\Sigma^+$, $A^2\Pi$, and $B^2\Sigma^+$ states were constructed as *morphed* functions of their *ab initio* counterparts $f^{ab}(r)$:

$$f^{morph}(r) = \alpha(r)[f^{ab}(r)-f_\infty]+f_\infty, \tag{12}$$

where f_∞ is the asymptotic value of the corresponding matrix element at the dissociation (atomic) limit [5]. The point-wise *ab initio* $f^{ab}(r_i)$ matrix elements taken from Terashkevich et al. [25] were interpolated using ordinary cubic splines with "natural" boundary conditions to construct continuous $f^{morph}(r)$ functions.

The radial functions, $\gamma_X(r)$ and $q_X(r)$, in Eq. (2) corresponding to the ground X-state were determined as

$$\gamma_X(r) = \alpha(r)\times\gamma^{ab}_X(r); \quad \gamma^{ab}_X(r) = \left[\sum_{j\in{}^2\Pi}\frac{2V^{so}_{Xj}L_{Xj}}{\Delta U_{Xj}}\right] \tag{13}$$

$$q_X(r) \equiv q^{ab}_X(r) = \sum_{j\in{}^2\Pi}\frac{|L_{Xj}|^2}{\Delta U_{Xj}} \tag{14}$$

where $\Delta U_{Xj}(r) = U_X(r) - U_j(r)$ and j iterates over higher lying $^2\Pi$ states except for the $A^2\Pi$ state. The required *ab initio* $\gamma^{ab}_X(r)$ and $q^{ab}_X(r)$ functions were borrowed from Ref. [25].

The "scaling" function, $\alpha(r)$, in Eqs. (12) and (13) was defined to be a linear function of the reduced coordinate $y_{p=1}(r)$ (see Eq. (11)):

$$\alpha(r) = \alpha_0 + \alpha_1\times y_{p=1}, \tag{15}$$

where the expansion coefficients, α_i, are adjusted fitting parameters with the initial values $\alpha_0 = 1$ and $\alpha_1 = 0$.

The Λ-doubling parameters corresponding to the $A^2\Pi$ state, $p_A(r)$, $q_A(r)$, $p_{A\Delta}(r)$, and $q_{A\Delta}(r)$ were approximated during the fit by the pure empirical function:

$$s(r) = s_0 + s_1\left[\frac{r/r_{\rm ref} - 1}{r/r_{\rm ref} + 1}\right], \tag{16}$$

where the initial values of the fitting coefficients s_0 and s_1 were taken to be a zero.

2.3. Fitting procedure

The trial set of electronic parameters of the RCC hamiltonian, that were included in the reduced 4×4 matrix of potential energies $\mathbf{V}^{e/f}(r;\mu,J)$, was iteratively refined during the non-linear minimization of the sum of squares: $\chi^2_{total}(\mathrm{a_p}) = \chi^2_{\rm exp} + \chi^2_{ab}$, where the first term is

$$\chi^2_{\rm exp} = \sum_{j=1}^{N^{\rm exp}_{fit}} \left(\frac{E^{\rm exp}_j + ZPE_{fit} - E^{CC}_j}{\sigma^{\rm exp}_j}\right)^2 \tag{17}$$

while the second one:

$$\chi^2_{ab} = \sum_i \sum_{k=1}^{N^{ab}} \left(\frac{U^{EMO}_i(r_k) - U^{ab}_i(r_k)}{\sigma^{ab}_i(r_k)}\right)^2 + \sum_j \sum_{k=1}^{N^{ab}} \left(\frac{f^{morph}_j(r_k) - f^{ab}_j(r_k)}{\sigma^{ab}_j(r_k)}\right)^2, \tag{18}$$

where $i \in [X^2\Sigma^+, A^2\Pi, B^2\Sigma^+]$, $j \in [A^{so}, V^{so}_{AB}, V^{so}_{AX}, L_{AB}, L_{AX}]$, and $\mathrm{a_p}$ are the non-linear fitting parameters of the global deperturbation model (2.1).

The experimental rovibronic termvalues, $E^{\rm exp}_j$, of the $X \sim A \sim B$ complex and their uncertainties, $\sigma^{\rm exp}_j$, were borrowed from Ref. [6]. The fitted zero-point-energy, $\mathrm{ZPE_{fit}}$, included in Eq. (17) is responsible for the uniform systematic shift of the origin of overall experimental term values. In the present work the ZPE-values correspond to the minimum of the ground X-state PEC.

The χ^2_{ab} term in the form of Eq. (18) was added to the conventional sum $\chi^2_{\rm exp}$ in order to provide the physically correct behavior of the electronic fitting parameters outside the current experimental region. The *ab initio* potentials, U^{ab}_i, and the corresponding electronic matrix elements $f^{ab}_j \in [A^{so}, V^{so}_{AB}, V^{so}_{AX}, L_{AB}, L_{AX}]$, were taken from Ref. [25], where they were provided as discrete functions of interatomic distance $r_k \in [0.85, 4.0]$ Å. Their uncertainties, $\sigma^{ab}(r_k)$, were determined as the residual of the relevant *ab initio* functions obtained using the alternative $aug-cc-pCV5Z$ and $aug-cc-pCV6Z$ atomic basis sets [33,34].

The minimum of the total $\chi^2_{total}(\mathrm{a_p}) = \chi^2_{\rm exp} + \chi^2_{ab}$ functional was found using the robust Levenberg-Marquardt algorithm realized in the MINPACK program suite [35]. The required Jacobian matrix was calculated numerically at each iteration using the central finite-difference (FD) schema. The overall number of fitting parameters, $\mathrm{a_p}$, could be as high as 65 depending on the deperturbation model used. The non-adiabatic eigenvalues, E^{CC}_j, were obtained using the iterative numerical solution of the 4×4 CC Eq. (1) defined on the interval $r \in [0.85; 2.85]$ Å. The corresponding band matrix was constructed using the five-points central FD approximation of the kinetic energy term in the radial Hamiltonian with a fixed number of grid points, $M = 1200$. The adaptive analytical mapping procedure [36] based on the reduced variable (11) with $p = 5$ and $r_{\rm ref} = 1.2$ Å parameters were implemented, together with an analytical extrapolation to zero step integration ($M \to \infty$) to minimize the truncation error in the resulting eigenvalues down to 0.001 $\mathrm{cm^{-1}}$.

Table 2
The rotationally averaged deviation of the calculated RCC, MoLList, and Duo (RCC/MoLList/Duo) rovibronic energies from the their experimental Marvel counterparts for the $X^2\Sigma^+$ state. $\Delta E^{\max} = \max|E^{Calc}_J - E^{MARVEL}_J|$. All deviations are in $\mathrm{cm^{-1}}$.

v_X	$J^{\max}_X$	Mean	RMSD	$\Delta E^{\max}$
0	97.5	-0.000/-0.01/-0.01	0.007/0.02/0.05	0.02/0.05/0.19
1	99.5	-0.000/-0.01/0.02	0.008/0.02/0.05	0.03/0.05/0.19
2	97.5	0.000/-0.01/0.01	0.009/0.02/0.06	0.04/0.03/0.21
3	81.5	0.001/-0.01/0.00	0.008/0.02/0.03	0.04/0.03/0.10
4	72.5	-0.000/-0.01/-0.02	0.007/0.02/0.04	0.05/0.05/0.14
5	60.5	-0.001/-0.01/-0.04	0.004/0.01/0.04	0.015/0.03/0.07
6	48.5	-0.000/-0.00/-0.04	0.004/0.01/0.04	0.016/0.05/0.05
7	36.5	-0.001/-0.01/0.03	0.004/0.01/0.03	0.01/0.03/0.05
8	34.5	-0.001/-0.01/0.01	0.004/0.01/0.03	0.015/0.03/0.06
9	30.5	0.001/-0.01/0.04	0.003/0.01/0.05	0.01/0.02/0.12
10	27.5	-0.003/-0.01/0.07	0.015/0.02/0.07	0.05/0.07/0.17
11	36.5	-0.006/0.59/0.10	0.14/1.89/0.19	0.36/5.93/0.57
12	19.5	-0.000/-0.00/0.05	0.008/0.02/0.06	0.02/0.05/0.11
13	23.5	0.02/-0.00/-0.04	0.15/0.10/0.12	0.72/0.52/0.53
14	37.5	0.19/0.03/-0.38	0.74/0.17/0.63	3.39/0.65/2.83
15	22.5	0.37/0.10/0.16	0.22/0.15/0.23	1.02/0.54/0.68
16	29.5	-0.20/ - /-0.51	0.30/ - /0.58	0.51/ - /0.99
17	32.5	0.85/ - /0.55	1.16/ - /1.22	3.39/ - /3.01
18	23.5	0.08/ - /-0.08	0.23/ - /0.22	0.77/ - /0.51

3. Results and discussion

3.1. Rovibronic term values of the $^{12}C^{14}N$ isotopomer

Three data sets of experimental rovibronic terms of the most abundant $^{12}C^{14}N$ isotopomer (see Table 1) were successively involved in the present RCC deperturbation analysis, which was realized utilizing the non-linear least squares fitting (NLSF) procedure described above. The first set (`set-I`) was restricted to the low vibrational quantum numbers: $v_X \in [0, 12]$, $v_A \in [0, 16]$, and $v_B \in [0, 10]$ of the treated states. The intermediate set (`set-II`) consisted of the $v_X \in [0, 18]$, $v_A \in [0, 22]$, and $v_B \in [0, 12]$ vibrational terms. The largest set (`set-III`) included all experimental term values available for $v_X \le 18$, $v_A \le 22$ and $v_B \le 19$ levels from the refined experimental MARVEL data [11]. The maximal rotational quantum numbers $J^{\max}$ were not limited in all sets above. $N^{\rm exp}_{total}$ is the total number of experimental term values belonging to each set, while $N^{\rm exp}_{fit}$ is the number of experimental term values actually included in the fitting procedure via Eq. (17). The number $N^{\rm exp}_{total} > N^{\rm exp}_{fit}$, since the term values with an experimental uncertainty $\sigma^{\rm exp}_j > 0.07$ $\mathrm{cm^{-1}}$ were excluded from the fit. The initial attempt to use these levels significantly degrades the fit. It seems the levels with $\sigma^{\rm exp}_j > 0.07$ $\mathrm{cm^{-1}}$ undergo the additional pronounced systematic error.

A comparison of the RMSDs obtained using the three experimental data sets are given in Table 1. The residuals of MARVEL experimental term values from the traditional EHA, Duo and the present RCC calculations for the $X^2\Sigma^+$, $A^2\Pi$ and $B^2\Sigma^+$ states are presented on Tables 2, 3 and 4, respectively. These values correspond to the residuals of individual rovibronic term values averaged within one vibrational level. Visual comparisons for the rovibronic terms predicted for each states of the complex in the framework of EHA and RCC models against the experimental energies from the `set-I` can be seen on Figs. 2, 3 and 4.

It can be clearly seen that the overall RMSD of 0.015 $\mathrm{cm^{-1}}$ obtained for `set-I` is comparable to the accuracy of the band-by-band EHA and is an order of magnitude better than the conventional Duo method (see, for instance, Fig. 3 of Ref. [22]). The vast majority of the calculated RCC energy levels are closer to their experimental counterparts than those generated using the perturbative EHA. The most significant improvement in level prediction by the RCC model, over the EHA, is observed for lowest locally

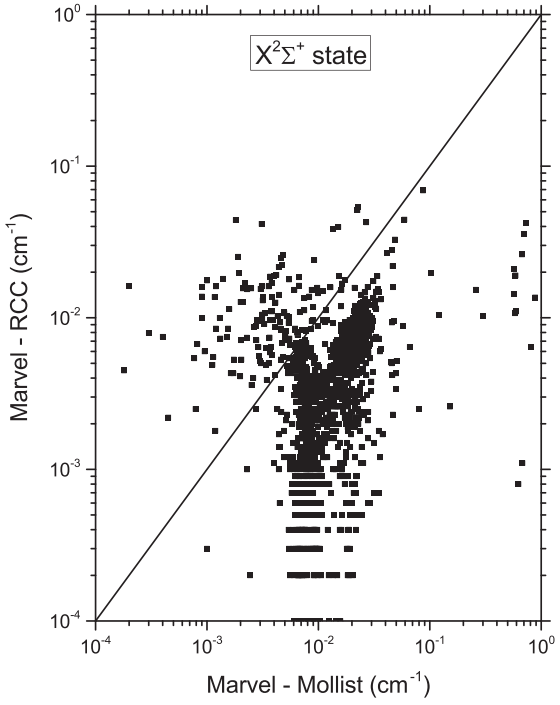

Fig. 2. Comparison of the residuals of MARVEL experimental term values from the traditional EHA (MoLList) and the present RCC calculations corresponding to the `set-I` of the ground state: $v_X \in [0, 12]$.

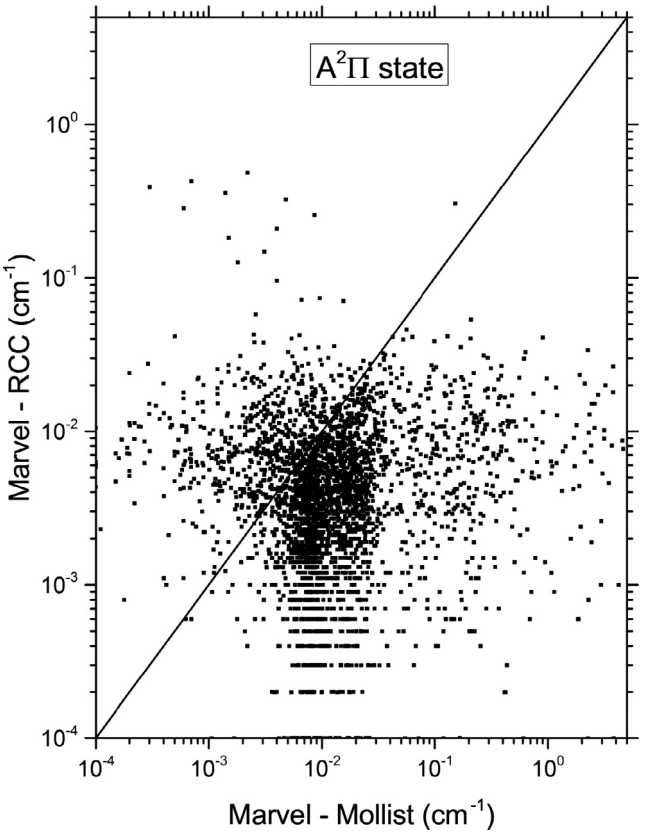

Fig. 3. Comparison of the residuals of MARVEL experimental term values from the traditional EHA (MoLList) and the present RCC calculations corresponding to the `set-I` of the $A^2\Pi$ state: $v_A \in [0, 16]$.

Table 3
The rotationally averaged deviation of the calculated RCC, MoLList, and Duo (RCC/MoLLit/Duo) rovibronic energies from the their experimental MARVEL counterparts for the $A^2\Pi$ state. $\Delta E^{\max} = \max|E_J^{Calc} - E_J^{MARVEL}|$. All deviations are in cm^{-1}.

v_A	$J_A^{\max}$	Mean	RMSD	$\Delta E^{\max}$
0	98.5	0.001/-0.01/-0.02	0.007/0.02/0.20	0.02/0.06/0.78
1	98.5	-0.001/-0.01/0.06	0.006/0.01/0.18	0.03/0.03/0.61
2	80.5	0.001/-0.01/0.07	0.012/0.01/0.14	0.19/0.04/0.36
3	99.5	-0.001/-0.02/0.00	0.006/0.11/0.15	0.03/1.14/0.47
4	97.5	0.001/-0.00/-0.05	0.008/0.08/0.16	0.06/0.98/0.41
5	94.5	0.001/-0.04/-0.06	0.010/0.30/0.17	0.05/3.14/0.45
6	82.5	0.001/-0.08/-0.06	0.010/0.41/0.17	0.04/3.83/0.47
7	37.5	0.001/-0.30/-0.05	0.066/1.15/0.11	0.17/4.82/0.27
8	41.5	-0.001/0.27/0.02	0.013/1.05/0.09	0.15/7.61/0.29
9	65.5	-0.001/-0.03/0.06	0.011/0.06/0.19	0.07/0.33/0.54
10	39.5	-0.005/-0.01/0.14	0.005/0.03/0.19	0.01/0.28/0.31
11	19.5	0.002/-0.01/0.21	0.007/0.01/0.24	0.03/0.02/0.35
12	22.5	0.001/-0.00/0.22	0.008/0.01/0.25	0.03/0.03/0.37
13	21.5	0.005/-0.01/0.20	0.008/0.01/0.23	0.03/0.03/0.36
14	20.5	0.003/-0.01/0.14	0.007/0.01/0.18	0.02/0.02/0.29
15	23.5	0.004/-0.00/0.05	0.008/0.02/0.11	0.03/0.19/0.19
16	24.5	-0.007/-0.01/-0.08	0.009/0.01/0.13	0.008/0.04/0.44
17	22.5	-0.002/0.01/0.08	0.01/0.16/0.67	0.04/0.60/3.15
18	23.5	-0.001/-0.00/-0.22	0.06/0.04/0.25	0.17/0.27/0.56
19	22.5	-0.006/-0.01/-0.30	0.013/0.01/0.33	0.01/0.06/0.62
20	19.5	0.003/-0.01/-0.26	0.01/0.01/0.34	0.04/0.04/0.94
21	21.5	-0.001/-0.01/0.03	0.02/0.02/0.27	0.03/0.13/0.40
22	20.5	0.001/-0.00/0.30	0.01/0.01/0.45	0.03/0.04/0.72

Table 4
The rotationally averaged deviation of the calculated RCC, MoLList, and Duo (RCC/MoLLit/Duo) rovibronic energies from the their experimental MARVEL counterparts for the $B^2\Sigma^+$ state. $\Delta E^{\max} = \max|E_J^{Calc} - E_J^{MARVEL}|$. All deviations are in cm^{-1}.

v_B	$J_B^{\max}$	Mean	RMSD	$\Delta E^{\max}$
0	63.5	0.003/-0.01/ 0.02	0.007/0.03/0.09	0.13/0.16/0.37
1	41.5	-0.016/-0.02/0.02	0.019/0.02/0.05	0.03/0.05/0.07
2	23.5	0.017/-0.02/1.20	0.014/0.03/1.28	0.04/0.07/1.72
3	22.5	0.015/0.11/-0.10	0.016/0.88/0.57	0.07/6.01/1.31
4	23.5	-0.009/-0.01/-1.16	0.010/0.02/1.27	0.01/0.05/2.23
5	24.5	-0.018/0.02/-1.91	0.024/0.37/2.09	0.065/1.71/3.72
6	25.5	-0.002/-0.01/-1.19	0.008/0.01/1.28	0.017/0.02/2.12
7	19.5	0.025/-0.05/0.22	0.082/0.12/0.35	0.47/0.52/1.60
8	26.5	0.011/-0.01/0.72	0.008/0.01/0.80	0.03/0.04/1.16
9	26.5	-0.023/-0.03/1.55	0.05/0.07/1.56	0.12/0.42/2.35
10	24.5	0.009/-0.00/0.84	0.013/0.09/1.03	0.06/0.33/2.03
11	36.5	-0.025/-0.05/0.51	0.19/0.13/1.23	0.29/0.63/6.43
12	15.5	-0.012/-0.04/-0.89	0.026/0.11/1.01	0.017/0.48/1.28
13	21.5	-0.015/-0.00/-2.00	0.03/0.02/2.00	0.06/0.05/2.12
14	37.5	-0.05/-0.08/-0.74	1.01/0.69/4.35	5.13/3.16/30.1
15	19.5	0.59/0.08/-0.20	0.06/0.13/0.31	0.73/0.500.62
16	37.5	-0.97/ - /2.66	2.45/ - /6.45	6.45/ - /38.0
17	30.5	-0.05/ - /3.34	1.59/ - /3.61	4.95/ - /7.18
18	33.5	0.58/ - /5.20	2.87/ - /7.30	13.9/ - /30.3
19	23.5	0.10/ - /0.22	0.12/ - /0.32	0.33/ - /0.94

perturbed $v_X = 11$, $v_A \in [3, 8]$, and $v_B = 0, 3, 5$ vibrational levels of the complex (see Table 5). Simultaneously, the present RCC model makes it possible to reproduce the entire fine structure of the complex with the almost spectroscopic accuracy. As expected, the most problematic vibrational levels in all deperturbation models are the highest ones, especially those belonging to the $B^2\Sigma^+$ state. It can be attributed to additional interaction with the "dark" quartet and sextet states manifold. Note that the fitted correction δ_{ZPE} to the total zero-point-energy ZPE_{fit} is found to be stably small, but not negligible, for all input sets.

3.2. Interatomic potentials

The resulting parameters of empirical EMO potentials derived for the $X^2\Sigma^+$, $A^2\Pi$, and $B^2\Sigma^+$ states of CN for `set-I` of the experimental term values are presented in Table 6. The alternative

Table 5
Extract from the output listing file corresponding to the experimental term values `set-I` and the mutually perturbed $A^2\Pi_{1/2}(v_A = 7) \sim X^2\Sigma^+(v_X = 11)$ f-parity rovibronic levels of $^{12}C^{14}N$. Full tables are available in the Supplemental materials. $\Delta = E^{exp} - E^{CC}$. All energies are in cm^{-1}, while the fractional partition P_i is in %.

$J+1/2$	E^{exp}	σ^{exp}	E^{CC}	Δ	$P_{A_{1/2}}$	$P_{A_{3/2}}$	P_X	P_B
1	22152.9498	0.0312	22152.9393	0.0105	99.7	0.0	0.3	0.0
2	22157.8303	0.0211	22157.8364	-0.0060	99.4	0.2	0.3	0.0
3	22165.9932	0.0150	22165.9925	0.0007	99.0	0.6	0.4	0.0
4	22177.4047	0.0068	22177.4051	-0.0004	98.5	1.2	0.4	0.0
5	22192.0705	0.0076	22192.0707	-0.0002	97.8	1.8	0.4	0.0
6	22209.9764	0.0139	22209.9852	-0.0089	97.0	2.6	0.4	0.0
7	22231.1440	0.0085	22231.1439	0.0001	96.1	3.5	0.4	0.0
8	22255.5414	0.0071	22255.5415	-0.0001	95.2	4.4	0.4	0.0
9	22283.1736	0.0080	22283.1725	0.0011	94.2	5.4	0.4	0.0
10	22314.0344	0.0052	22314.0313	0.0032	93.1	6.5	0.4	0.0
11	22348.1140	0.0083	22348.1119	0.0021	92.0	7.5	0.5	0.0
12	22385.4127	0.0048	22385.4086	0.0041	90.9	8.6	0.5	0.0
13	22425.9194	0.0048	22425.9157	0.0037	89.8	9.7	0.5	0.0
14	22469.6336	0.0049	22469.6275	0.0061	88.7	10.7	0.6	0.0
15	22516.5425	0.0049	22516.5386	0.0039	87.6	11.8	0.6	0.0
16	22566.6497	0.0049	22566.6438	0.0059	86.5	12.8	0.7	0.0
17	22619.9439	0.0049	22619.9383	0.0056	85.4	13.8	0.8	0.0
18	22676.4232	0.0049	22676.4176	0.0057	84.4	14.8	0.9	0.0
19	22736.0840	0.0049	22736.0777	0.0063	83.3	15.7	1.0	0.0
20	22798.9222	0.0049	22798.9157	0.0065	82.2	16.6	1.2	0.0
21	22864.9369	0.0054	22864.9302	0.0068	81.1	17.4	1.5	0.0
22	22934.1273	0.0054	22934.1221	0.0052	80.0	18.1	1.9	0.0
23	23006.5035	0.0054	23006.4980	0.0055	78.6	18.8	2.6	0.0
24	23082.0812	0.0054	23082.0761	0.0051	76.9	19.2	3.9	0.0
25	23160.9100	0.0060	23160.9053	0.0048	74.3	19.2	6.5	0.0
26	23243.1358	0.0060	23243.1307	0.0051	68.6	18.2	13.2	0.0
27	23329.2507	0.0060	23329.2415	0.0092	53.1	14.1	32.8	0.0
28	23411.4969	0.0069	23411.4946	0.0024	51.4	17.4	31.2	0.0
29	23503.9219	0.0060	23503.9213	0.0007	66.6	22.2	11.2	0.0
30	23598.6782	0.0069	23598.6711	0.0071	71.1	24.1	4.8	0.0
31	23696.2519	0.0085	23696.2595	-0.0076	72.4	25.1	2.5	0.0
32	23796.8497	0.0120	23796.8412	0.0085	72.7	25.8	1.5	0.0

Table 6
The resulting fitted parameters of the EMO potential energy curves (defined by the Eqs. (9)–(11)) for the $X^2\Sigma^+$, $A^2\Pi$, and $B^2\Sigma^+$ states of CN obtained using `set-I` of experimental term values (see Table 1). T_e is the electronic term, D_e is the dissociation energy are given in cm^{-1}, the equilibrium bond lengths, r_e, and the reference distance, r_{ref}, are given in Å. The polynomial expansion coefficients, β_i are dimensionless. $p = 3$ and $N = 11$ for all states. The symbol ‡ marks the fixed parameters.

	$X^2\Sigma^+$	$A^2\Pi$	$B^2\Sigma^+$
T_e	‡0.0	9244.990	25753.268
D_e	‡62800.0	53555.010	56276.424
r_e	1.1717581432	1.2328109635	1.1512467113
‡r_{ref}	1.2	1.4	1.2
β_0	2.5661841875	2.4711516802	2.8428969376
β_1	0.3131893375	0.3072809872	0.3192612426
β_2	0.4000377522	0.4215078990	-0.4943078572
β_3	0.4082731310	0.4759502604	-2.2708079658
β_4	0.6117640276	0.5758112596	-7.2050711568
β_5	0.7904831415	0.5231053751	-23.4328121497
β_6	0.0439995268	0.5343730971	0.0895487135
β_7	0.9040290061	0.0013014662	221.1275319867
β_8	8.3341106959	-1.9048447097	218.7315527295
β_9	-0.0059200320	-2.4795165771	-720.6420260873
β_{10}	-16.7936431296	-0.0024682491	-549.9897275429
β_{11}	13.5541978986	0.0001605346	994.9287021111

Table 7
The resulting fitted parameters of the EMO potential energy curves (defined by the Eqs. (9)–(11)) for the $X^2\Sigma^+$, $A^2\Pi$, and $B^2\Sigma^+$ states of CN obtained using `set-II` of experimental term values (see Table 1). T_e is the electronic term, D_e is the dissociation energy are given in cm^{-1}, the equilibrium bond lengths, r_e, and the reference distance, r_{ref}, are given in Å. The polynomial expansion coefficients, β_i are dimensionless. $p = 3$ and $N = 11$ for all states. The symbol ‡ marks the fixed parameters.

	$X^2\Sigma^+$	$A^2\Pi$	$B^2\Sigma^+$
T_e	‡0.0	9244.977	25753.303
D_e	‡62800.0	53554.997	56276.389
r_e	1.1717566069	1.2325912020	1.1512540586
‡r_{ref}	1.2	1.4	1.2
β_0	2.5662285705	2.4712196994	2.8430062880
β_1	0.3108303801	0.3074053839	0.3214099993
β_2	0.4021595795	0.4210878161	-0.5089112484
β_3	0.5272110175	0.4779785895	-2.3070618533
β_4	0.4821817698	0.5921043055	-6.9391183259
β_5	-0.5540577244	0.5023281633	-23.7889536523
β_6	-0.3051241007	0.4081872717	0.0103354345
β_7	-1.1730128576	0.0001074838	229.1497599253
β_8	53.7322037048	-1.8420243127	198.0057727766
β_9	0.1373774983	-2.7077295959	-745.5697268135
β_{10}	-275.2562159084	0.0000256700	-466.7768528456
β_{11}	282.1395321217	-0.0027726883	953.8342605062

EMO parameters obtained for `set-II` and `set-III` are given in Tables 7 and 8, respectively. The corresponding EMO PECs can be seen on Fig. 1.

The required initial set of EMO parameters for the isolated (deperturbed) X, A, and B states were obtained during the NLSF of a merged set of the respective point-wise empirical (Rydberg-Klein-Rees) [26,37] and *ab initio* potentials [25]. The electronic term $T_e(X) \equiv 0$ and dissociation energy $D_e(X)$ of the ground X-state were both fixed during the fit. The value D_e(X)=62800.0 (in cm^{-1}) is the *ab initio* estimate from Ref. [25]. The electronic terms of the excited A and B states were constrained as $T_e(A) = D_e(X) - D_e(A)$ and $T_e(B) = D_e(X) - D_e(B) + \Delta E$, respectively. Here, $\Delta E = E_{2_D}(N) - E_{4_S}(N) = 19229.6\ cm^{-1}$ is the difference of the experimental nitrogen terms [38] (see Fig. 1). The dissociation energies of the excited states, $D_e(A)$ and $D_e(B)$, as well as the equilibrium distance, r_e, and polynomial coefficients, β_i, were treated as adjusted fitting parameters of the EMO potential, whereas p and r_{ref} parameters were fixed (see Section 2.3 for details). For each of the electronic states, a dozen expansion coefficients, β, appearing in Eq. (10) turned out to be sufficient. The equilibrium parameters

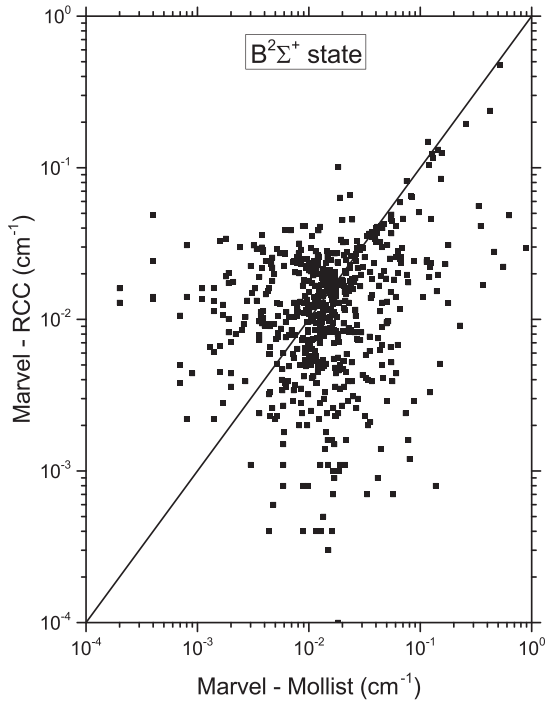

Fig. 4. Comparison of the residuals of MARVEL experimental term values from the traditional EHA (MoLList) and the present RCC calculations corresponding to the `set-I` of the $B^2\Sigma^+$ state: $v_B \in [0, 10]$).

Table 8
The resulting fitted parameters of the EMO potential energy curves (defined by the Eqs. (9)–(11)) for the $X^2\Sigma^+$, $A^2\Pi$, and $B^2\Sigma^+$ states of CN obtained using `set-III` of experimental term values (see Table 1). T_e is the electronic term, D_e is the dissociation energy are given in cm^{-1}, the equilibrium bond lengths, r_e, and the reference distance, r_{ref}, are given in Å. The polynomial expansion coefficients, β_i are dimensionless. $p = 3$ and $N = 11$ for all states. The symbol ‡ marks the fixed parameters.

	$X^2\Sigma^+$	$A^2\Pi$	$B^2\Sigma^+$
T_e	‡0.0	9245.005	25753.606
D_e	‡62800.0	53554.982	56276.752
r_e	1.1717555034	1.2327700637	1.1512176850
‡r_{ref}	1.2	1.4	1.2
β_0	2.5661027061	2.4711811388	2.8422538104
β_1	0.3145503689	0.3072409694	0.2923449444
β_2	0.4039728728	0.4196612220	-0.3211634660
β_3	0.1891128708	0.4851495934	-1.2383046312
β_4	1.0083521985	0.6303722209	-13.2275002738
β_5	8.7213169677	0.4290056433	-38.0908930460
β_6	-21.4577463705	0.0001739374	77.0282917319
β_7	-92.5389676528	0.0002708831	309.1082236918
β_8	326.7620724001	-0.3415171811	-169.1125209557
β_9	199.1686195517	-1.0576679839	-935.3697396234
β_{10}	-1405.8239120908	0.0006740631	30.8321202452
β_{11}	1123.1322205501	-0.0058020396	1193.0110454954

and the lowest β_i-coefficients of the EMO potentials were found to be rather stable with respect to input term values set, whereas the higher order β_i - coefficients expectedly demonstrate a high variability (compare β_i-values in Tables 6, 7, and 8).

The resulting EMO potentials for all states of the $X \sim A \sim B$ complex deviate of from their empirical RKR analogues up to a few tens of cm^{-1} across the experimental energy region available

Table 9
A comparison of the electronic terms, T_e, the dissociation energies, D_e, and the equilibrium distances, r_e, obtained for the $X^2\Sigma^+$, $A^2\Pi$, and $B^2\Sigma^+$ states of CN using alternative deperturbation procedures and direct *ab initio* calculation. RCC - reduced coupled-channel deperturbation analysis performed in the present work; EHA - conventional effective Hamiltonian approach (EHA) [18]; Duo - the conventional CC deperturbation analysis [22] accomplished in the framework of Duo program [21]; Expt. - experimental measurement [7]; *ab initio* - first principles electronic structure calculation [14]. The electronic term of the ground state was fixed at zero for all methods.

	$X^2\Sigma^+$	$A^2\Pi$	$B^2\Sigma^+$	Source
T_e/cm^{-1}	0.0	9244.991(15)	25753.4(3)	RCC
	0.0	9243.296(5)	25752.59(1)	EHA
	0.0	9246.87	25755.6	Duo
	0.0	9109.95	25776.4	*ab initio*
D_e/cm^{-1}	62800.0 [25]	53555.00(2)	56276.5(3)	RCC
	62588.6			Expt.
	63619.4	63619.4	57087.5	Duo
	63077.4	53968.2	56659.5	*ab initio*
r_e/Å	1.171757(2)	1.23272(9)	1.15123(2)	RCC
	1.1718063(9)	1.2330449(9)	1.15133(12)	EHA
	1.17272	1.23135	1.14979	Duo
	1.1714	1.2324	1.151	*ab initio*

for each state. Outside of the experimental data region, the EMO PECs of the ground and first excited states also agree very well with their *ab initio* counterparts [25]. However, the EMO potential of the $B^2\Sigma^+$ state demonstrates a noticeable deviation from the *ab initio* potential at large internuclear distances, probably due to its non-regular character.

Table 9 compares the equilibrium spectroscopic constants obtained for the present EMO PECs with previous empirical and *ab initio* data, including those used to generate the MoLList (EHA) and EXOMOL (Duo) lists, respectively. The present equilibrium constants for all states are closest to their their EHA counterparts. The extremely small difference between the EHA and RCC constants are likely to be responsible for a high accuracy of the RCC energy levels.

3.3. Spin-orbit and L-uncoupling matrix elements

The resulting spin-orbit and *L*-uncoupling electronic matrix elements responsible for the SO splitting of the $A^2\Pi$ state and the overall non-adiabatic interactions in the $X \sim A \sim B$ complex are depicted on Figs. 5 and 6. The open squares on both figures denote the previous empirical values from Refs. [15,16]. The adjusted $\alpha_0 \approx 1$ and $\alpha_1 \approx 0$ coefficients of the scaling function (15), used for morphing the *ab initio* SO and *L*-uncoupling functions [25] in accordance with Eq. (12), are given in Table 10.

In general, both SO and *L*-uncoupling matrix elements demonstrate a very weak sensitivity to the particular set of input experimental energies of the complex used in the NLSF fitting. Across the sets, the *L*-uncoupling functions are found to be most stable. The maximal deviation of the fitting L_{AX} and L_{AB} functions from their *ab initio* counterparts in the entire *r*-range $r \in [0.7, 4.0]$ Å do not exceed 0.01 and 0.04 *a.u.*, respectively (see Fig. 6). All morphed electronic matrix elements are remarkably close to their empirical counterparts, which were previously extracted from locally perturbed levels of the complex using the traditional band-by-band EHA. The most significant residual (reaching up 1–2 cm^{-1} at small and intermediate distances) is observed for the diagonal SO splitting, A^{so}, function (see Fig. 5).

There is also a very good agreement of the present empirical A^{so} and V_{AX}^{so} functions with their *ab initio* counterparts evaluated previously in Ref. [5] since a maximal discrepancy observed over the entire range of internuclear distances does not really exceed few reciprocal centimeters. It should be noted that the asymptotic values of A^{so}, V_{AX}^{so} and L_{AX} functions estimated in [5] were used as

Table 10
The fitted parameters of the scaling $\alpha(r)$ function (15) used for morphing the *ab initio* SO and *L*-uncoupling electronic matrix elements in Eq. (12) as well as the *ab initio* γ_X-splitting function in Eq. (13) for the ground state. The dimensionless coefficients $\alpha_{0,1}$ were obtained during the NLSF of the three I/II/III experimental term value sets. The asymptotic f_∞-values were fixed at their atomic counterparts [5].

	A^{so}	V^{so}_{AX}	V^{so}_{AB}
α_0	1.0452/1.0454/1.0453	1.0326/1.0329/1.0270	1.0045/1.0075/0.9886
α_1	-0.0590/-0.0709/-0.0613	-0.0005/0.0003/0.0210	0.0002/-0.0000/-0.0002
f_∞/cm^{-1}	-4.66	+6.59	0.0
	L_{AX}	L_{AB}	γ_X
α_0	1.0066/1.0068/1.0064	0.9712/0.9810/0.9858	1.32/0.94/1.14
α_1	0.0000/0.0004/0.00005	-0.0184/-0.0073/0.0001	-2.97/19.9/6.59
f_∞/*a.u.*	$-\sqrt{2}$	0.0	-

Table 11
The coefficients of the empirical $s(r)$ function (16) used to represent the Λ-doubling parameters of the $A^2\Pi$ state. The s_0 and s_1 coefficients were obtained during the NLSF of the three (I/II/III) experimental term value sets. The *ab initio* values were calculated at the equilibrium point $r_e(A)$ using the relevant point-wise functions available in Ref. [25]. The p_A and $p_{A\Delta}$ are dimensionless, while q_A and $q_{A\Delta}$ in 1/cm^{-1}.

	$p_A \times 10^{-4}$	$p_{A\Delta} \times 10^{-4}$	$q_A \times 10^{-5}$	$q_{A\Delta} \times 10^{-5}$
s_0	-4.23/-4.60/-4.20	-4.8/-12.5/-0.77	-2.32/-2.20/-2.16	-16.0/-36.7/-3.6
s_1	0.185/0.024/-0.102	248.0/300.9/255.8	-17.2/-19.7/-22.5	-83.5/-126.0/-57.0
ab initio	-5.4	-0.81	-2.2	-5.7

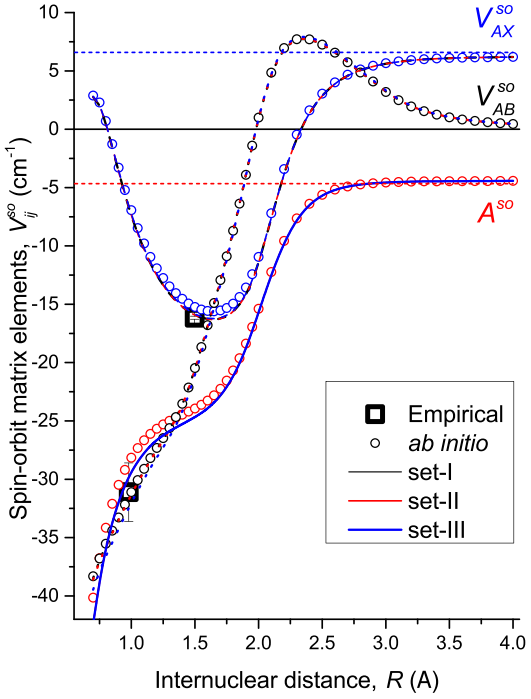

Fig. 5. Comparison of the morphed diagonal and off-diagonal SO electronic matrix elements $A^{so}(r)$, $V^{so}_{AX}(r)$ and $V^{so}_{AB}(r)$ obtained in the present work as a result of the RCC fitting of the three experimental data sets (`set I-III`) with respect to the MARVEL term values [11]. *Ab initio* data was borrowed from Ref. [25] while empirical data was taken from Refs. [15,16]. The red and blue horizontal lines mark the asymptotic values $A^{so}(r \to +\infty) \to -4.66$ and $V^{so}_{AX}(r \to +\infty) \to +6.59$ (in cm^{-1}), respectively. The corresponding asymptotic value of the $V^{so}_{AB}(r)$ function is zero. In according to Ref. [5], asymptotic values $A^{so}(r)$ and $V^{so}_{AX}(r)$ functions obey the relationship: $V^{so}_{AX} = -\sqrt{2}A^{so}$. (For interpretation of the references to colour in this figure legend, the reader is referred to the web version of this article.)

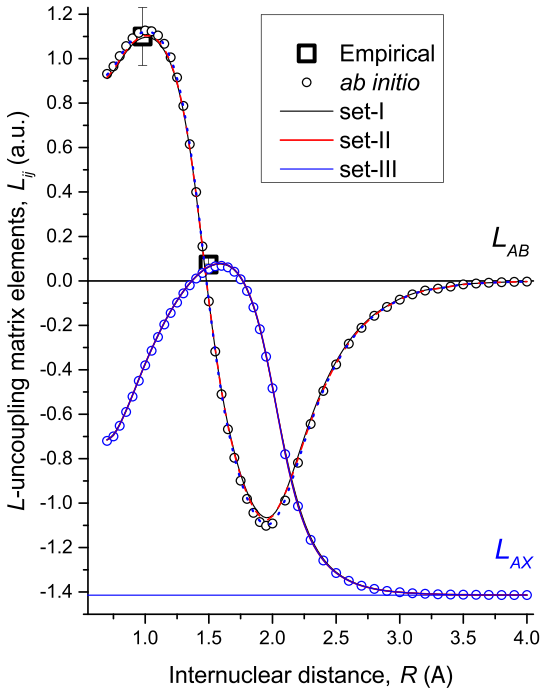

Fig. 6. Comparison of the morphed *L*-uncoupling electronic matrix elements $L_{AX}(r)$ and $L_{AB}(r)$ obtained as a result of the RCC fitting completed in the present work for the three sets (`set I-III`) of the MARVEL experimental term values [11]. The corresponding *ab initio* data is taken from Ref. [25] while empirical data from Refs. [15,16]. The blue horizontal line marks the asymptotic value $L_{AX}(r \to +\infty) \to -\sqrt{2}$ (in *a.u.*) according to Ref. [5]. The corresponding asymptotic value of the $L_{AB}(r)$ function is zero. (For interpretation of the references to colour in this figure legend, the reader is referred to the web version of this article.)

the asymptotic f_∞ parameters in Eq. (12) to constrain the corresponding functions at $r \to +\infty$ (see Figs. 5, 6 and Table 10).

3.4. Fine structure parameters

The s_0 and s_1 fitting coefficients derived for the pure empirical Λ-doubling functions of the $A^2\Pi$ state are presented in Table 11. The adjusted parameters of the scaling function, $\alpha(r)$, used for morphing the *ab initio* $\gamma_X(r)$ function in Eq. (13) for the ground X-state are given in Table 11 as well. Recall that the radial function $q_X(r)$ (see Eq. (14) was fixed at its *ab initio* counterpart, $q^{ab}_X(r)$, from Terashkevich et al. [25] while the relevant $\gamma_B(r)$ and $q_B(r)$ functions of the excited $B^2\Sigma^+$ state were completely neglected in the present model.

The present empirical $p_A(r)$ and $q_A(r)$ functions are found to be an order of magnitude less than their experimental Λ-doubling counterparts obtained for the lowest $v_A \in [0, 6]$ vibrational levels of the $A^2\Pi$ state in the framework of the traditional EHA [37]. At

the same time, the fitted $\gamma_X(r)$ function from Eq. (13) is only 2-2.5 times smaller than the corresponding experimental $\gamma_X(v)$-values derived for the lowest $v_X \in [0, 10]$ levels of the ground state [39].

All empirically obtained fine structure parameters demonstrate a high volatility with respect to the particular experimental term values used (see details in Table 11). The most pronounced variations are observed for the $p_{A\Delta}$ and $q_{A\Delta}$ functions arisen from the interaction of the $A^2\Pi$ state with the higher-lying $^2\Delta$ state manifold. It means that the empirical Λ-doubling parameters of the $A^2\Pi$ state have predominantly a phenomenological character in contrast to their counterparts for the ground state. Nevertheless, the present fully empirical s_0 values still reasonably agree with their *ab initio* counterparts.

3.5. Line positions of the minor isotopologues

It should be emphasized that all parameters of the modeling Hamiltonian in Section 2.1 explicitly depend on the reduced molecular mass. Furthermore, both the adjusted and fixed electronic parameters of the present RCC model are supposed to be mass-invariant functions of interatomic distance. This is not technically true, since the *L*-uncoupling matrix elements theoretically depend on the location of the molecular center mass [13]. However, this possible μ-dependence is assumed too weak for observation.

To validate mass-invariant properties of the resulting deperturbation parameters adjusted above using solely the most abundant $^{12}C^{14}N$ isotopologue data, were used as a line list for predicting the rotational, vibrational and rovibronic transitions which are also observed for minor $^{13}C^{14}N$ and $^{12,13}C^{15}N$ isotopologues. This has been done simply by substituting for the proper reduced mass in Eq. (1).

For the lowest $J = 1.5 - 0.5$ and $J = 2.5 - 1.5$ pure rotational, i.e. neglecting the hyperfine structure, transitions corresponding to $v_X \in [0, 9]$ vibrational levels of both e/f components of the ground $X^2\Sigma^+$ state of $^{13}C^{14}N$ isotopologue the predicted *R*-line positions coincided with their MW spectroscopic counterparts to within 10^{-4} cm^{-1}. In fact, this is the same accuracy as that of the EHA. For the rotational-vibrational transitions corresponding to the fundamental $1 - 0$ band the theoretical P/R line positions ($J \in [4, 27]$) represent their experimental IR counterparts with a RMSD of about 0.004 cm^{-1} and a systematic shift (Exp. - Calc.) of +0.001, +0.007, and +0.01 cm^{-1} for the $^{12}C^{15}N$, $^{13}C^{15}N$, and $^{13}C^{14}N$ isotopologues, respectively.

In the case of the $A - X$ and $B - X$ electronic transitions, a systematic divergence of the theoretical rovibronic line positions from the corresponding experimental data is much more pronounced (see, for example, Table 12). However, this mainly concerns the so-called electronic and vibrational isotopic shifts, whereas the *J*-dependence of the observed deviations are normally very weak. This means that the rotational molecular constants derived in the framework of the present RCC analysis, including fine structure functions, are indeed mass-invariant. The isotopic shifts of the $A - X$ bands weakly depend on vibrational excitation, while the analogues shifts of the $B - X$ bands slightly increase as v_B-values increase. The main part of the electronic shifts observed in both $A - X$ and $B - X$ systems seem to be attributed to a mass-depended adiabatic correction, which is tacitely hidden in the present empirical PECs.

The observed v-dependance of the $B - X$ shift can be caused by non-adiabatic coupling taking place within $^2\Sigma^+$ states manifold. The recent *ab initio* electronic structure calculations [25] indeed claim that the radial coupling matrix element between $B^2\Sigma^+$ and $X^2\Sigma^+$ states is significant in the entire range of interatomic distances. Therefore, the electronic coupling between the $B^2\Sigma^+$ and $X^2\Sigma^+$ states was explicitly accounted for the present RCC model by introducing the non-vanishing off-diagonal matrix element, $V^{el}_{XB}(r)$, which is responsible for the electrostatic interaction of diabatic states. However, the resulting empirical $V^{el}_{XB}(r)$ function was found to be unexpectedly small for all input sets. We attribute the observed discrepancy to the supposition that the *J*-independent electrostatic interaction is already included implicitly (at least in part through the empirical PECs) within the present deperturbation model.

Table 12
Systematic shifts (Mean) and RMSD values (in cm^{-1}) extracted from the residual of experimental line positions from their theoretical counterparts belonging to several bands of the $A - X$ and $B - X$ systems of $^{13}C^{14}N$ and $^{12}C^{15}N$ isotopologues. The line positions were predicted in the framework of the present RCC model using the `set-I` of the mass-invariant structure parameters.

Band	J^{max} $^{13}C^{14}N$	Mean	RMSD	J^{max} $^{12}C^{15}N$	Mean	RMSD
$A - X$ system						
0–1	82.5	-0.209	0.006	48.5	-0.135	0.004
1–2	50.5	-0.221	0.006	48.5	-0.146	0.004
2–4	52.5	-0.230	0.006	43.5	-0.144	0.005
3-1	64.5	-0.218	0.007	34.5	-0.149	0.008
4-2	52.5	-0.221	0.006	46.5	-0.154	0.010
$B - X$ system						
0-0	39.5	-0.055	0.014	46.5	-0.03	0.02
1–2	34.5	-0.106	0.016	30.5	-0.05	0.02
2–3	30.5	-0.100	0.035			
3–4	22.5	-0.114	0.008			
4-4	23.5	-0.155	0.012			
5-4	23.5	-0.185	0.012			

4. Concluding remarks

A direct global deperturbation analysis of the 5600–6570 experimental rovibronic term values belonging to the $X^2\Sigma^+$, $A^2\Pi$ and $B^2\Sigma^+$ states of the most abundant $^{12}C^{14}N$ isotopologue has been performed in the framework of the reduced 4×4 coupled-channel deperturbation model utilizing analytical potential energy curves as well as *ab initio* spin-orbit and *L*-uncoupling electronic matrix elements between all states of the $X \sim A \sim B$ complex. The explicit treatment the residual perturbations of the complex caused by the excited states has significantly improved accuracy of the description of the *A*-state. It has been shown that the regular intramolecular interaction of the complex with the excited states manifold insets about 30–40% into the experimental γ_X-splitting of the ground *X*-state and contributes almost nothing into its γ_B counterpart of the excited *B*-state.

The present RCC deperturbation analysis is based on following important items: (i) reliable experimental data set obtained by MARVEL procedure, (ii) high level electronic structure calculations including the conventional PECs, spin-orbit and *L*-uncoupling non-adiabatic matrix elements, (iii) introducing into the RCC model additional radial functions responsible for the regular coupling with the remote states manifold, (iv) non-empirical estimates of the fine structure parameters by means of the 2-nd order van-Vleck transformation, (v) usage of the *ab initio* estimates to regularize the inverted RCC problem.

The optimized interatomic potentials, electronic SO and *L*-un coupling functions, together with the fine structure radial functions, describe the vast majority of the experimental term values of both locally and regularly perturbed levels of the $X \sim A \sim B$ complex with the RMSD value of 0.015-0.05 cm^{-1}, which is comparable or even better than the accuracy achieved in the framework of the traditional effective Hamiltonian approach. The resulting mass-invariant deperturbed parameters generate rotational and rovibrational spectral lines of all CN isotopologues with the almost spectroscopic accuracy. The rovibronic line positions predicted for both the $A - X$ and $B - X$ transitions of the minor isotopologues demonstrate a small systematic shift which very weakly depends on vi-

brational and rotational quantum numbers. We believe that the robust RCC deperturbation model could significantly extend the rovibronic line-list of the CN radical to a wide region of vibrational and rotational quantum numbers, which are inevitably excited under high (probably non-equilibrium) temperature conditions.

Acknowledgment

The work was supported by the Russian Science Foundation (RSF) (grant No.22-23-00272).

Declaration of Competing Interest

The authors declare that they have no known competing financial interests or personal relationships that could have appeared to influence the work reported in this paper.

CRediT authorship contribution statement

V.A. Terashkevich: Investigation, Formal analysis, Methodology, Validation. **E.A. Pazyuk:** Conceptualization, Methodology, Validation, Visualization. **A.V. Stolyarov:** Conceptualization, Project administration, Writing – review & editing, Writing – original draft. **S.N. Yurchenko:** Conceptualization, Methodology, Writing – review & editing.

Supplementary material

Supplementary material associated with this article can be found, in the online version, at doi:10.1016/j.jqsrt.2022.108366.

References

[1] McKellar A. Evidence for the molecular origin of some hitherto unidentified interstellar lines. Publ Astron Soc Pac 1940;52(307):187. doi:10.1086/125159.
[2] Leach S. Why COBE and CN spectroscopy cosmic background radiation temperature measurements differ, and a remedy. Mon Not R Astron Soc 2012;421(2):1325–30. doi:10.1111/j.1365-2966.2011.20390.x.
[3] Fray N, Bénilan Y, Cottin H, Gazeau M-C, Crovisier J. The origin of the CN radical in comets: a review from observations and models. Planet Space Sci 2005;53(12):1243–62. doi:10.1016/j.pss.2005.06.005.
[4] Ritchey AM, Federman SR, Lambert DL. Interstellar CN AND CH^+ in diffuse molecular clouds:$^{12}C/^{13}C$ ratios and CN excitation. Astrophys J 2011;728(1):36. doi:10.1088/0004-637x/728/1/36.
[5] Antipov SV, Gustafsson M, Nyman G. Spin-orbit and rotational couplings in radiative association of $C(^3P)$ and $N(^4S)$ atoms. J Chem Phys 2011;135(18):184302. doi:10.1063/1.3562125.
[6] Syme A-M, Mousley A, Cunningham M, McKemmish LK. Diatomic rovibronic transitions as potential probes for proton-to-electron mass ratio across cosmological time. Aust J Chem 2020;73:743–56. doi:10.1071/CH19448.
[7] Huang Y, Barts SA, Halpern JB. Heat of formation of the cyanogen radical. J Phys Chem 1992;96(1):425–8. doi:10.1021/j100180a079.
[8] Baudelet M, Guyon L, Yu J, Wolf J-P, Amodeo T, Fréjafon E, et al. Spectral signature of native CN bonds for bacterium detection and identification using femtosecond laser-induced breakdown spectroscopy. Appl Phys Lett 2006;88(6):063901. doi:10.1063/1.2170437.
[9] Tran M, Sun Q, Smith BW, Winefordner JD. Determination of C/H/O/N ratios in solid organic compounds by laser-induced plasma spectroscopy. J Anal At Spectrom 2001;16:628–32. doi:10.1039/B009905H.
[10] Furtenbacher T, Csaszar A, Tennyson J. Marvel: measured active rotational–vibrational energy levels. J Mol Spectrosc 2007;245:115–25. doi:10.1016/j.jms.2007.07.005.
[11] Syme A-M, McKemmish LK. Experimental energy levels of $^{12}C^{14}N$ through Marvel analysis. Mon Not R Astron Soc 2020;499(1):25–39. doi:10.1093/mnras/staa2791.
[12] Van Vleck JH. On σ-Type doubling and electron spin in the spectra of diatomic molecules. Phys Rev 1929;33:467–506. doi:10.1103/PhysRev.33.467.
[13] Lefebvre-Brion H, Field RW. The spectra and dynamics of diatomic molecules: revised and enlarged edition. Academic Press; 2004.
[14] Yin Y, Shi D, Sun J, Zhu Z. Transition dipole moments and transition probabilities of the CN radical. Astrophys J Suppl Ser 2018;235(2):25. doi:10.3847/1538-4365/aab26b.
[15] Kotlar AJ, Field RJ, Steinfeld J, Coxon JA. Analysis of perturbations in the $A^2\Pi$–$X^2\Sigma^+$ æredg system of CN. J Mol Spectrosc 1980;80:86–108.
[16] Ito H, Kazama A, Kuchitsu K. Perturbations in the CN($B^2\Sigma^+ - X^2\Sigma^+$) tail band system Part 4. The $B^2\Sigma^+ \sim A^2\Pi$ perturbations in the v_B = 11, 14–16, 18 and 19 levels. J Mol Struct 1994;324(1):29–43. doi:10.1016/0022-2860(94)08223-5.
[17] Brown JM, Colbourn EA, Watson JKG, Wayne FD. An effective Hamiltonian for diatomic molecules: *ab initio* calculations of parameters of HCl^+. J Mol Spectrosc 1979;74(2):294–318. doi:10.1016/0022-2852(79)90059-6.
[18] Brooke JSA, Ram RS, Western CM, Li G, Schwenke DW, Bernath PF. Einstein a coefficients and oscillator strengths for the $A^2\Pi$–$X^2\Sigma^+$ (Red) and $B^2\Sigma^+$–$X^2\Sigma^+$ (Violet) systems and rovibrational transitions in the $X^2\Sigma^+$ state of CN. Astrophys J Suppl Ser 2014;210(2):23. doi:10.1088/0067-0049/210/2/23.
[19] Roy RJL. LEVEL: A computer program for solving the radial Schrödinger equation for bound and quasibound levels. J Quant Spectrosc Radiat Transf 2017;186:167–78. doi:10.1016/j.jqsrt.2016.05.028.
[20] Western CM. PGOPHER: a program for simulating rotational, vibrational and electronic spectra. J Quant Spectrosc Radiat Transf 2017;186:221–42. doi:10.1016/j.jqsrt.2016.04.010.
[21] Yurchenko SN, Lodi L, Tennyson J, Stolyarov AV. Duo: a general program for calculating spectra of diatomic molecules. Comput Phys Commun 2016;202:262–75. doi:10.1016/j.cpc.2015.12.021.
[22] Syme A-M, McKemmish LK. Full spectroscopic model and trihybrid experimental-perturbative-variational line list for CN. Mon Not R Astron Soc 2021;505(3):4383–95. doi:10.1093/mnras/stab1551.
[23] Kozlov SV, Pazyuk EA, Stolyarov AV. A reduced method of coupled vibrational channels: analysis of regular perturbations in the $c^3\Sigma_u^+$-State of a KRb molecule. Opt Spectrosc 2018;125(4):464–9. doi:10.1134/S0030400X18100119.
[24] Havalyova I, Bozhinova I, Pashov A, Ross AJ, Crozet P. A coupled–channels model describing the low-lying $^2\Delta$, $^2\Sigma^+$ and $^2\Pi$ electronic states of nickel monohydride with experimental accuracy. J Quant Spectrosc Radiat Transf 2021;272:107800. doi:10.1016/j.jqsrt.2021.107800.
[25] Terashkevich VA, Pazyuk EA, Stolyarov AV. A computational study of the non-adiabatic coupling among low-lying doublet states of the CN radical. J Quant Spectrosc Radiat Transf 2021;276:107916. doi:10.1016/j.jqsrt.2021.107916.
[26] Ram R, Davis S, Wallace L, Engleman R, Appadoo D, Bernath P. Fourier transform emission spectroscopy of the $B^2\Sigma^+$–$X^2\Sigma^+$ system of CN. J Mol Spectrosc 2006;237:225–31. doi:10.1016/j.jms.2006.03.016.
[27] Ivanova M, Pashov ASaA, Stolyarov A, Knöeckel H, Tiemann E. The $X^2\Sigma^+$ state of LiCa studied by Fourier-transform spectroscopy. J Chem Phys 2011;135(17):174303. doi:10.1063/1.3652755.
[28] Mizushima M. The theory of rotating diatomic molecules. Wiley New York; 1975.
[29] Ozaki Y, Ito H, Suzuki K, Kondow T, Kuchitsu K. Rotational perturbations in the CN ($B^2\Sigma^+$-$X^2\Sigma^+$) tail band system. II. Identification of the CN($^4\Pi$) state and its vibrational levels. Chem Phys 1983;80(1):85–94. doi:10.1016/0301-0104(83)85170-2.
[30] Ito H, Ozaki Y, Suzuki K, Kondow T, Kuchitsu K. Emission spectrum of the CN($B^2\Sigma^+ - X^2\Sigma^+$) tail band system: $B^2\Sigma^+ \sim^4 \Pi$ perturbations in the v_B=9, 12, and 17 levels. J Chem Phys 1992;96(6):4195–204. doi:10.1063/1.462838.
[31] Le Roy Robert L. dPotFit: a computer program to fit diatomic molecule spectral data to potential energy functions. J Quant Spectrosc Radiat Transfer 2017;186:179–96. doi:10.1016/j.jqsrt.2016.06.002.
[32] Šurkus AA, Rakauskas RJ, Bolotin AB. The generalized potential energy function for diatomic molecules. Chem Phys Lett 1984;105(3):291–4. doi:10.1016/0009-2614(84)85032-0.
[33] Dunning TH. Gaussian basis sets for use in correlated molecular calculations. I. The atoms boron through neon and hydrogen. J Chem Phys 1989;90:1007–23. doi:10.1063/1.456153.
[34] Woon DE, Dunning TH. Gaussian basis sets for use in correlated molecular calculations. V. Core-valence basis sets for boron through neon. J Chem Phys 1995;103(11):4572–85. doi:10.1063/1.470645.
[35] More J, Garbow B, Hillstrom K. MINPACK software for solving nonlinear equations and nonlinear least squares problems. University of Chicago, Argonne National Laboratory; 1999.
[36] Meshkov VV, Stolyarov AV, Le Roy RJ. Adaptive analytical mapping procedure for efficiently solving the radial Schrödinger equation. Phys Rev A 2008;78:052510. doi:10.1103/PhysRevA.78.052510.
[37] Ram R, Wallace L, Bernath PF. High resolution emission spectroscopy of the $A^2\Pi$–$X^2\Sigma^+$ "red" system of $^{12}C^{14}N$. J Mol Spectrosc 2010;263:82–8. doi:10.1016/j.jms.2010.07.002.
[38] Kramida A, Ralchenko Y, Reader J. and NIST ASD Team NIST atomic spectra database (ver. 5.8). Gaithersburg, MD: National Institute of Standards and Technology; 2020. [Online]. Available: https://physics.nist.gov/asd[2021, July 29]
[39] Terashkevich VA, Pazyuk EA. Nature of the fine structure of rotational levels of the ground $X^2\Sigma^+$-State of the radical CN. Opt Spectrosc 2021;129(1):12–17. doi:10.1134/S0030400X21010185.